Pulsed-Beam Propagation in Dispersive Media via Pulsed Plane Wave Spectral Decomposition

Timor Melamed and Leopold B. Felsen, *Life Fellow, IEEE*

Abstract—This paper is concerned with the behavior of transient wavefields due to a pulsed-beam (PB) wavepacket launched obliquely from a hypothetical aperture plane in a medium with generic dispersion $k(\omega)$, where k and ω are wavenumber and frequency, respectively. This generalizes our previous investigation of a PB launched normally from the hypothetical aperture plane. The problem is solved through spectral decomposition into plane waves in the frequency (ω) and spatial wavenumber ($\boldsymbol{\xi}$) domains, followed by asymptotics on the spectral inversion integrals, with ω synthesis performed *before* $\boldsymbol{\xi}$ synthesis. Special attention in the transient spectral domain is given to paraxial PB approximations and to criteria for their range of validity, which are expressed in terms of critical nondimensional estimators that contain the beam parameters as well as the dispersion parameters of the medium. The resulting PB's can be used to synthesize transient wavefields excited by *arbitrary space–time* source distributions of finite support on a specified aperture plane in the medium.

Index Terms—Dispersive media, pulsed beam.

I. INTRODUCTION

WE INVESTIGATE here the propagation properties of a pulsed-beam (PB) wavepacket launched obliquely from a hypothetical aperture plane into a lossless dispersive homogeneous unbounded medium characterized generically by the frequency (ω)-dependent ambient wavenumber $k(\omega)$. The motivation and direct time-domain (TD) solution strategy having been outlined in the abstract, we proceed directly to the contents that follow. The presentation is based on several previous studies [1]–[3] to which we refer for background. To make the paper reasonably self contained, we summarize those previous results that are relevant to the understanding of the present results. In particular, we follow the same sequence of steps as in the analysis of the nontilted PB [3] in order to facilitate assessment of the tilt effect here, although this may involve similar wording in the two texts. The problem is formulated in Section II, with definition of the frequency and wavenumber spectral transforms, the paraxial PB spectral initial conditions, and the spectral synthesis of the resulting paraxial TD-PB field in the dispersive

medium. Section III has a summary of the corresponding results for the nondispersive case $k(\omega) = \omega/c$, which can be evaluated in closed form and permits assessment of the effects of dispersion developed by the asymptotics in Section IV. The dispersive asymptotic plane wave spectrum for the PB initial conditions, obtained by frequency-domain (FD) saddle-point techniques, is parameterized in terms of the saddle point (stationary) frequencies $\tilde{\omega}_s$, which depend on space–time (r, t) as well as PB tilt $\bar{\boldsymbol{\xi}}$, spectral spread $\boldsymbol{\xi}$, and pulse length T. These parameters are combined in various nondimensional descriptors that furnish criteria for the domain of validity of the paraxially approximated PB. The detailed derivation and interpretation of these criteria, and the corresponding comparisons with the nondispersive and nontilted dispersive results in [1]–[3] constitute the principal new contributions in this paper. These spectral footprints are retained in subsequent asymptotics associated with a spectral synthesis that leads to the final space–time tilted paraxial PB at the end of Section IV. Brief conclusions are presented in Section V.

II. FORMULATION OF THE PROBLEM

The problem of PB wavepacket propagation in a lossless, homogeneous, isotropic dispersive medium is defined by the PB matched initial distribution in the FD and is Fourier inverted from there into the TD.

A. Time-Frequency Transforms

The Fourier transforms

$$\hat{u}(r, \omega) = \int_{-\infty}^{\infty} u(r, t)e^{i\omega t}\, dt \tag{1a}$$

$$u(r, t) = \frac{1}{2\pi} \int_{-\infty}^{\infty} \hat{u}(r, \omega)e^{-i\omega t}\, d\omega \tag{1b}$$

with $r = (x_1, x_2, z)$ denoting conventional Cartesian coordinates, define the relations between a TD field $u(r, t)$ and the corresponding FD field $\hat{u}(r; \omega)$. Here and henceforth, a caret $\hat{}$ identifies FD wave fields. To accommodate wave constituents with evanescent (i.e., complex) spectra as encountered in the PB, it is useful to employ the analytic signal formulation for TD fields. The analytic field $\overset{+}{u}(r, t)$ (denoted by the symbol $^+$) corresponding to the FD field $\hat{u}(r, \omega)$ is obtained by the one-sided inverse Fourier transform

$$\overset{+}{u}(r, t) = \frac{1}{\pi} \int_{0}^{\infty} \hat{u}(r, \omega)e^{-i\omega t}\, d\omega, \qquad \text{Im}\, t \leq 0 \tag{2}$$

where $\hat{u}(r, \omega)$ is defined in (1a). The real field is given by

$$u(r, t) = \text{Re}\, \overset{+}{u}(r, t). \tag{3}$$

B. Space-Wavenumber Transforms

Space-wavenumber transforms are required to decompose fields into plane waves parameterized by their spectral wavenumbers. If $\hat{u}_o(\boldsymbol{x}, \omega)$ is the FD distribution corresponding to the TD initial distribution $u_o(\boldsymbol{x}, t)$ for the PB on the $z = 0$ plane, then the corresponding FD wavenumber spectral amplitude on the initial surface is given by

$$\hat{\tilde{u}}_o(\boldsymbol{\xi}, \omega) = \int_{-\infty}^{\infty} d^2x \, \hat{u}_o(\boldsymbol{x}, \omega) e^{-ik(\omega)\boldsymbol{\xi} \cdot \boldsymbol{x}} \qquad (4a)$$

with $\boldsymbol{x} = (x_1, x_2)$, $\sim$ identifying a wavenumber spectral function, $\boldsymbol{\xi} = (\xi_1, \xi_2)$ denoting the normalized (with respect to k) spatial wavenumber vector, and $k(\omega)$ denoting the generic frequency-dependent wavenumber in the ambient medium. The FD initial field is reconstructed as

$$\hat{u}_o(\boldsymbol{x}, \omega) = [k(\omega)/2\pi]^2 \int d^2\xi \, \hat{\tilde{u}}_o(\boldsymbol{\xi}, \omega) e^{ik(\omega)\boldsymbol{\xi} \cdot \boldsymbol{x}}. \qquad (4b)$$

The ω dependence of $k = k(\omega)$ and of $\hat{u}(\boldsymbol{r}) = \hat{u}(\boldsymbol{r}, \omega)$ will be suppressed unless specifically required for clarity. Also, integration limits are omitted on all integrals extending from $-\infty$ to $+\infty$. The plane-wave synthesis of the FD field away from the initial plane is obtained by including the plane wave spectral propagator $\exp(ik\zeta z)$

$$\hat{u}(\boldsymbol{r}, \omega) = [k/2\pi]^2 \int d^2\xi \, \hat{\tilde{u}}_o(\boldsymbol{\xi}) e^{ik(\boldsymbol{\xi} \cdot \boldsymbol{x} + \zeta z)} \qquad (5)$$

where

$$\zeta = \sqrt{1 - \xi^2}, \quad \xi^2 \equiv \boldsymbol{\xi} \cdot \boldsymbol{\xi}, \quad \text{Im} \, \zeta \geq 0. \qquad (6)$$

Inserting (5) into (2) yields the formal plane wave spectral representation of the TD analytic field at any observation point $\boldsymbol{r}$

$$\overset{+}{u}(\boldsymbol{r}, t) = \frac{1}{\pi} \int_0^{\infty} d\omega \left[\frac{k(\omega)}{2\pi} \right]^2 \int d^2\xi \, \hat{\tilde{u}}(\boldsymbol{\xi}, \omega) e^{-i\omega t + ik(\omega)\overset{\circ}{\boldsymbol{\kappa}} \cdot \boldsymbol{r}}$$
$$(7)$$

where $\overset{\circ}{\boldsymbol{\kappa}} = (\boldsymbol{\xi}, \zeta)$ is the unit vector along the direction of propagation of the spectral plane wave.

C. PB Initial Distribution

To facilitate space–time focusing of the PB wavefield in the dispersive environment, it is useful to specify FD "iso-diffracting" initial distributions such that the focusing distance is independent of frequency (see [4]),

$$\hat{u}_o(\boldsymbol{x}, \omega) = \exp[-\tfrac{1}{2} k(\omega)\beta^{-1} \boldsymbol{x}^2 + ik\overline{\boldsymbol{\xi}} \cdot \boldsymbol{x} - \tfrac{1}{2} \omega T] \qquad (8)$$

where
$\boldsymbol{x}^2 \equiv \boldsymbol{x} \cdot \boldsymbol{x}$,
$T > 0$ (for $\omega > 0$) smoothing parameter;
$\beta = \beta_r + i\beta_i$
(with $\beta_r > 0$
for $\omega > 0$)
frequency-independent parameter;
$\overline{\boldsymbol{\xi}} = (\overline{\xi}_1, \overline{\xi}_2)$ spectral parameter which determines the beam axis tilt, with respect to initial plane $z = 0$ [see also (16)].

In [4], the initial distribution was defined for a *nondispersive* medium with $k = \omega/c$. The generalization in (8) to arbitrary $k(\omega)$ requires a dispersion-matched k-dependent initial field in order to retain the iso-diffracting property. Insertion of (8) into (4a) yields the corresponding plane wave spectrum

$$\hat{\tilde{u}}_0(\boldsymbol{\xi}, \omega) = (2\pi\beta/k) \exp[-\tfrac{1}{2} k\beta(\boldsymbol{\xi} - \overline{\boldsymbol{\xi}})^2 - \tfrac{1}{2} \omega T]. \qquad (9)$$

The spectral shift $\overline{\boldsymbol{\xi}}$ introduced in (8) and (9) parameterizes the general class of PB's whose axis is *tilted* with respect to the initial distribution plane $z = 0$. Such PB's are required for decomposition of arbitrary planar "aperture field" distributions into pulsed beam basis functions [5], [6] and their consideration constitutes the generalization of the nontilted results in [1]–[3]. Regarding $\hat{u}_o(\boldsymbol{x}, \omega)$ as a function of ω, the *on-axis* ($\boldsymbol{x} = 0$) distribution in (8) peaks at $\omega = 0$ where $\hat{u}_o = 1$. Therefore, the maximum frequency of the on-axis signal may be estimated by solving $\exp(-1/2) = \exp(-\omega T/2)$, giving $\omega_{\max} \simeq T^{-1}$. Such a band-limited pulse may be regarded as a model for a physical (sampled) signal. By applying the inverse transform (2) to (8), one obtains the PB initial distribution $u_o(\boldsymbol{x}, t) = \text{Re} \, \overset{+}{u}_o(\boldsymbol{x}, t)$, with

$$\overset{+}{u}_o(\boldsymbol{x}, t) = \int_0^{\infty} d\omega$$
$$\cdot \exp\left[-i\omega\left(t - \frac{i}{2}T\right) + ik(\omega)\left(\overline{\boldsymbol{\xi}} \cdot \boldsymbol{x} + \frac{i}{2}\beta^{-1}\boldsymbol{x}^2\right) \right] \quad (10)$$

D. TD Wavefield

In [1] and [2], the TD field was evaluated and interpreted via the space–time spectral representation in (7), following the conventional route in which one first performs the spatial wavenumber synthesis in the FD and thereafter the inversion to the TD. The analysis was carried out for a nontilted z-directed propagating beam with $\overline{\boldsymbol{\xi}} = 0$ in the initial distribution (8). In [3], the order of integration in (7) was inverted, evaluating the ω-integral first, thereby obtaining the wavenumber spectral representation

$$\overset{+}{u}(\boldsymbol{r}, t) = \int d^2\xi \, \overset{+}{\tilde{u}}(\boldsymbol{r}, t; \boldsymbol{\xi}) \qquad (11)$$

wherein the spectral wave functions $\overset{+}{\tilde{u}}(\boldsymbol{r}, t; \boldsymbol{\xi})$ are dispersive transient plane waves

$$\overset{+}{\tilde{u}}(\boldsymbol{r}, t; \boldsymbol{\xi}) = \frac{1}{\pi} \int_0^{\infty} d\omega \left[\frac{k(\omega)}{2\pi} \right]^2 \hat{\tilde{u}}_0(\boldsymbol{\xi}, \omega) e^{-i\omega t + ik(\omega)\overset{\circ}{\boldsymbol{\kappa}} \cdot \boldsymbol{r}}.$$
$$(12)$$

III. NONDISPERSIVE CASE

To assess the influence of dispersion on the PB behavior, we summarize for later comparison the previously obtained results pertaining to the nondispersive case $k(\omega) = \omega/c$ [5], [6], [7].

A. PB Initial Distribution

The nondispersive TD initial distribution is given by (10) with $k(\omega) = \omega/c$, giving

$$u_o(\boldsymbol{x}, t) = \text{Re } \overset{+}{u}_o(\boldsymbol{x}, t)$$
$$= \text{Re } \overset{+}{\delta}\left[t - \frac{i}{2}T - c^{-1}\left(\frac{1}{2}\beta^{-1}\boldsymbol{x}^2 - i\overline{\boldsymbol{\xi}} \cdot \boldsymbol{x} \right) \right] \tag{13}$$

where $\overset{+}{\delta}(t) = 1/\pi i t$ is the analytic δ function defined in the lower half of the complex t-plane.

B. PB Wavefield and Paraxial Asymptotics

Inserting $k(\omega) = \omega/c$ into (12), we obtain the nondispersive TD spectral plane wave

$$\overset{+}{u}(\boldsymbol{r}, t; \boldsymbol{\xi}) = \frac{1}{\pi}\int_0^\infty d\omega \left[\frac{\omega}{2\pi c} \right]^2 \hat{\overset{+}{u}}_0(\boldsymbol{\xi}, \omega)e^{-i\omega[t - c^{-1}\overset{\circ}{\boldsymbol{\kappa}} \cdot \boldsymbol{r}]}. \tag{14}$$

For the Gaussian initial distribution in (8), inserting (9) into (14) yields

$$\overset{+}{u}(\boldsymbol{r}, t; \boldsymbol{\xi}) = \frac{i\beta}{2\pi c}\overset{+}{\delta}{}'\left[t - \frac{i}{2}T - c^{-1}\left(\overset{\circ}{\boldsymbol{\kappa}} \cdot \boldsymbol{r} + \frac{i}{2}\beta(\boldsymbol{\xi} - \overline{\boldsymbol{\xi}})^2 \right) \right] \tag{15}$$

where the prime denotes the derivative with respect to the argument, i.e., $\overset{+}{\delta}{}'(t) = -1/(\pi i t^2)$. Since the analytic signal decays with the increase of the negative imaginary part of its argument, the most strongly excited spectral plane wave in (15) is the one with $\boldsymbol{\xi} = \overline{\boldsymbol{\xi}}$ where the transient plane wave delay function has the form $t - (i/2)T - c^{-1}\overset{\circ}{\boldsymbol{\kappa}} \cdot \boldsymbol{r}$. The corresponding preferred propagation (i.e., beam axis) direction is along the unit vector

$$\overset{\circ}{\boldsymbol{\kappa}} = (\overline{\boldsymbol{\xi}}, \overline{\zeta}), \qquad \overline{\zeta} = \sqrt{1 - \overline{\boldsymbol{\xi}}^2}. \tag{16}$$

Inserting (15) into (11), we obtain for the spectrally synthesized PB

$$\overset{+}{u}(\boldsymbol{r}, t) = \frac{i\beta}{2\pi c}\int d^2\xi$$
$$\overset{+}{\delta}{}'\left[t - \frac{i}{2}T - c^{-1}\left(\overset{\circ}{\boldsymbol{\kappa}} \cdot \boldsymbol{r} + \frac{i}{2}\beta(\boldsymbol{\xi} - \overline{\boldsymbol{\xi}})^2 \right) \right]. \tag{17}$$

The abovementioned localization of the integrand about $\boldsymbol{\xi} = \overline{\boldsymbol{\xi}}$ facilitates the approximate evaluation of the integral, which leads to the paraxial PB field

$$\overset{+}{u}(\boldsymbol{r}, t) = \sqrt{\frac{\det \boldsymbol{Q}(z)}{\det \boldsymbol{Q}(0)}}$$
$$\cdot \overset{+}{\delta}\left[t - \frac{i}{2}T - c^{-1}\left(z_b + \frac{1}{2}\boldsymbol{x}_b \cdot \boldsymbol{Q} \cdot \boldsymbol{x}_b \right) \right] \tag{18}$$
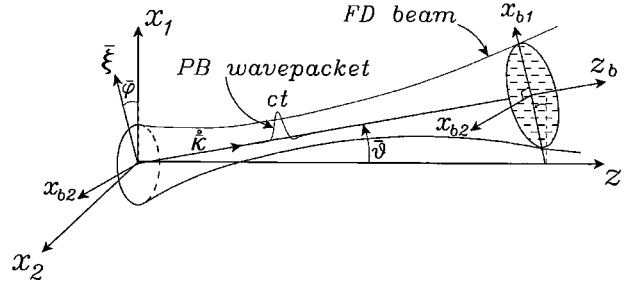
Fig. 1. The beam field in configuration space, with axis z_b along the $\overset{\circ}{\boldsymbol{\kappa}}(\overline{\vartheta}, \overline{\varphi})$ direction. The transverse beam coordinates (x_{b_1}, x_{b_2}), defined in (20), are such that x_{b_1} lies in the plane $(\overline{\boldsymbol{\xi}}, \overset{\circ}{\boldsymbol{\kappa}})$, where x_{b_2} is parallel to the z-plane. The PB wavepacket adapts locally to the transverse profile of the FD beam.

where

$$\boldsymbol{Q} = \begin{bmatrix} (z\overline{\zeta}^{-1} - i\beta\overline{\zeta}^2)^{-1} & 0 \\ 0 & (z\overline{\zeta}^{-1} - i\beta)^{-1} \end{bmatrix}. \tag{19}$$

Equation (18) is written in terms of the beam-centered coordinates (x_{b_1}, x_{b_2}, z_b) defined for specified $\overline{\boldsymbol{\xi}}$ by the transformation

$$\begin{bmatrix} x_{b_1} \\ x_{b_2} \\ z_b \end{bmatrix} = \begin{bmatrix} \cos\overline{\vartheta}\cos\overline{\varphi} & \cos\overline{\vartheta}\sin\overline{\varphi} & -\sin\overline{\vartheta} \\ -\sin\overline{\varphi} & \cos\overline{\varphi} & 0 \\ \sin\overline{\vartheta}\cos\overline{\varphi} & \sin\overline{\vartheta}\sin\overline{\varphi} & \cos\overline{\vartheta} \end{bmatrix} \begin{bmatrix} x_1 \\ x_2 \\ z \end{bmatrix} \tag{20}$$

where $(\overline{\vartheta}, \overline{\varphi})$ are the spherical angles that define the beam direction $\overset{\circ}{\boldsymbol{\kappa}} = (\overline{\boldsymbol{\xi}}, \overline{\zeta})$ (Fig. 1)

$$\cos\overline{\vartheta} = \overline{\zeta}, \quad \cos\overline{\varphi} = \overline{\xi}_1/|\overline{\boldsymbol{\xi}}|, \quad \sin\overline{\varphi} = \overline{\xi}_2/|\overline{\boldsymbol{\xi}}|. \tag{21}$$

Here, the z_b coordinate lies along the beam axis whereas x_{b_1} and x_{b_2} are orthogonal coordinates in planes perpendicular to z_b. In view of (19), the quadratic form $\boldsymbol{x}_b \cdot \boldsymbol{Q} \cdot \boldsymbol{x}_b$ in (18) is given by $x_{b_1}^2 Q_{11} + x_{b_2}^2 Q_{22}$. Thus, the transverse coordinate frame $\boldsymbol{x}_b = (x_{b_2}, x_{b_1})$ is oriented so that x_{b_1} lies in the plane $(\overline{\boldsymbol{\xi}}, \overset{\circ}{\boldsymbol{\kappa}})$ (see Fig. 1).

The main properties of the PB field in (18) (discussed in detail in [7], [6]) are as follows.

1) The tilted PB is astigmatic [7]. In a conventional $\overline{\boldsymbol{\xi}} = 0$ PB, the elements of $\boldsymbol{Q}$ depend only on z_b, i.e., on the location *along* the beam axis, whereas here they depend on $z = \overline{\zeta}z_b - |\overline{\boldsymbol{\xi}}|x_{b_1}$. This difference is due to the fact that the $\overline{\boldsymbol{\xi}} = 0$ paraxial initial conditions are given on a plane normal to the beam axis, whereas here they are defined on a plane of constant z, which is generally inclined with respect to the beam axis. It follows that (18) conforms smoothly with the initial field distribution $u_o(\boldsymbol{x}, t)$ on the $z = 0$ plane.

2) For large enough z_b, we may replace $z\overline{\zeta}^{-1} = z_b - x_{b_1}\tan\overline{\vartheta} \simeq z_b$, so that $\boldsymbol{Q}$ is simplified and (18) changes gradually into a conventional PB. This motivates rewriting the elements of $\boldsymbol{Q}$ in (19) in the form

$$Q_{jj} = (z_b - Z_j - iF_j)^{-1} \equiv 1/R_j + i/I_j \tag{22}$$

where for $j = 1$ or 2, $R_j(z_b)$ is given by $R_j = (z_b - Z_j) + F_j^2/(z_b - Z_j)$, $Z_1 = -\beta_i \overline{\zeta}^2$, $F_1 = \beta_r \overline{\zeta}^2$, $Z_2 = -\beta_i$, $F_2 = \beta_r$, and $I_j(z_b) = F_j(1 + (z_b - Z_j)^2/F_j^2)$. The PB field in (18) may now be written as an astigmatic PB whose major axes are oriented along x_{b_1} and x_{b_2}

$$\overset{+}{u}(\mathbf{r},\, t) = \sqrt{\frac{(-Z_1 - iF_1)(-Z_2 - iF_2)}{(z_b - Z_1 - iF_1)(z_b - Z_2 - iF_2)}}$$
$$\cdot \overset{+}{\delta}\left[t - t_p(\mathbf{r}) - \frac{i}{2} T_p(\mathbf{r}) \right] \tag{23}$$

where $t_p(\mathbf{r}) = c^{-1}(z_b + x_{b_1}^2/2R_1 + x_{b_2}^2/2R_2)$, $T_p(\mathbf{r}) = T + c^{-1}(x_{b_1}^2/I_1 + x_{b_2}^2/I_2)$.

In (23), $t_p(\mathbf{r})$ is the paraxial propagation delay along the z_b axis, while R_j are the wavefront principal radii of curvature in the x_{b_j} directions [see (23)]. $T_p(\mathbf{r})$ is the temporal half-amplitude length of the $\overset{+}{\delta}$ pulse, which is inversely proportional to the pulse amplitude. Thus, the PB field is strongest on the beam axis where $T_p(\mathbf{r})$ is minimal and the field decays as T_p increases away from the beam axis. The half-amplitude beam width in the x_{b_j} directions is found by solving $T_p(\mathbf{x}_{b_j}) = 2T_p(0)$, giving $D_j(z_b) = 2\sqrt{cTI_j(z_b)}$. The collimation lengths in the (x_{b_j}, z_b) cross-sectional planes are F_j and the waists are located at $z_b = Z_j$ with the corresponding widths $2\sqrt{cTF_j}$. From (23) with (22), one notes that in the collimation (Fresnel) zone $|z_b - Z_j| < F_j$, the PB profile is essentially unchanged, whereas outside this zone the beam spreads and its profile approaches the far-field diffraction angles (asymptotes) $\Theta_j = 2\sqrt{cT/F_j}$.

IV. DISPERSIVE CASE

A. Transient Plane Wave Spectrum

1) Formal Solution and Asymptotics: The TD spectral constituents excited by the FD PB initial distribution in (8) with (9) are given formally by inserting (9) into (12)

$$\overset{+}{u}(\mathbf{r},\, t;\, \boldsymbol{\xi}) = \frac{1}{\pi} \int_0^\infty d\omega\, \beta k(\omega) e^{-i\Phi(\mathbf{r}\, t;\, \boldsymbol{\xi}\, \omega)}, \quad \mathrm{Im}\, t \le 0 \tag{24}$$

$$\Phi(\mathbf{r},\, t;\, \boldsymbol{\xi},\, \overline{\boldsymbol{\xi}};\, \omega,\, T) = \omega\left(t - \frac{i}{2} T \right) - k(\omega)\tilde{S}$$

$$\tilde{S}(\boldsymbol{\xi},\, \mathbf{r}) = \overset{\circ}{\boldsymbol{\kappa}} \cdot \mathbf{r} + \frac{i}{2}\beta(\boldsymbol{\xi} - \overline{\boldsymbol{\xi}})^2. \tag{25}$$

Except when required for clarity, we shall not include in the notation all of the parameters in the argument of Φ. The integral in (24) is evaluated asymptotically by continuing the integrand analytically into the complex ω-plane and applying the saddle-point method. The stationary frequency $\tilde{\omega}_s$ satisfies the relation $(d\Phi/d\omega) = 0$ at $\tilde{\omega}_s$, so that using (25)

$$\frac{t - \dfrac{i}{2} T}{\tilde{S}} = k'(\tilde{\omega}_s), \quad \tilde{\omega}_s = \tilde{\omega}_s(\mathbf{r},\, t;\, \boldsymbol{\xi},\, \overline{\boldsymbol{\xi}};\, T) \tag{26}$$

where the prime denotes differentiation with respect to ω. The field in (24) is approximated asymptotically by the lowest order saddle-point formula [8]

$$\int B(\omega;\, \mathbf{r},\, t) e^{-i\Phi(\omega;\, \mathbf{r},\, t)}\, d\omega \sim \left[\frac{2\pi}{i\Phi''(\tilde{\omega}_s;\, \mathbf{r},\, t)} \right]^{1/2}$$
$$\cdot B(\tilde{\omega}_s;\, \mathbf{r},\, t) e^{-i\Phi(\tilde{\omega}_s;\, \mathbf{r},\, t)}, \quad \Phi'(\tilde{\omega}_s) = 0 \tag{27}$$

to yield

$$\overset{+}{u}(\mathbf{r},\, t;\, \boldsymbol{\xi}) \sim \overset{+}{\tilde{A}}(\mathbf{r},\, t;\, \boldsymbol{\xi}) e^{-i\tilde{\Psi}(\mathbf{r},\, t,\, \boldsymbol{\xi})} \tag{28}$$

with the spectral phase and the amplitude given by [recall that $\tilde{\omega}_s$ depends on all the parameters shown in (26)]

$$\tilde{\Psi}(\mathbf{r},\, t;\, \boldsymbol{\xi},\, \overline{\boldsymbol{\xi}}) \equiv \Phi(\mathbf{r},\, t;\, \boldsymbol{\xi},\, \tilde{\omega}_s,\, T)$$
$$= \left(t - \frac{i}{2} T \right) \tilde{\omega}_s - k(\tilde{\omega}_s)\tilde{S}, \tag{29}$$

$$\overset{+}{\tilde{A}}(\mathbf{r},\, t,\, \boldsymbol{\xi},\, \overline{\boldsymbol{\xi}}) = \beta k(\tilde{\omega}_s)[-2\pi i\tilde{S}k''(\tilde{\omega}_s)]^{-1/2}. \tag{30}$$

Equation (26) requires the analytic continuation of the dispersion relation $k(\omega)$ into the complex ω plane. The equation has a real solution $\overline{\omega}_s$ if the following three conditions are simultaneously satisfied: 1) $T = 0$ (temporal impulse); 2) $\boldsymbol{\xi} = \overline{\boldsymbol{\xi}}$ (propagation along the beam axis); and 3) only for propagating beams with $\overline{\boldsymbol{\xi}} < 1$. These conditions ensure that the resulting $\tilde{S} = \overset{\circ}{\boldsymbol{\kappa}} \cdot \mathbf{r} = z_b$ is real. Instead of solving (26) formally, we shall take advantage of the spatial localization of the Gaussian PB. Since the spatially evanescent part of the spectrum in (9) along the transverse off-axis coordinates is proportional to $\exp[-(1/2)k(\omega)\beta(\boldsymbol{\xi} - \overline{\boldsymbol{\xi}})^2]$, the main contribution to the field is obtained from the $\boldsymbol{\xi} \approx \overline{\boldsymbol{\xi}}$ spectral constituents. Also we assume that T is a "small" parameter; the smallness requirement is quantified later on [see (50) and (51)]. For $\boldsymbol{\xi} \approx \overline{\boldsymbol{\xi}}$ and small T values, we now define $\overline{\omega}_s(\mathbf{r},\, t;\, \overline{\boldsymbol{\xi}})$ as the stationary *real* frequency of the field in (28) for *on-axis* observation points $(z_b,\, t) = (\overset{\circ}{\boldsymbol{\kappa}} \cdot \mathbf{r},\, t)$

$$c\frac{dk}{d\omega}\bigg|_{\omega = \overline{\omega}_s} = \overline{\Omega}, \quad \overline{\Omega} \equiv \frac{ct}{z_b} = \frac{ct}{\overset{\circ}{\boldsymbol{\kappa}} \cdot \mathbf{r}}. \tag{31}$$

As noted earlier, $z_b = \overset{\circ}{\boldsymbol{\kappa}} \cdot \mathbf{r}$ is real for $|\overline{\boldsymbol{\xi}}| < 1$. Moreover, $z_b = ct$ defines the wavefront of the PB field and $z_b < ct$ defines on-axis points behind the wavefront. Interpretation of (31) is facilitated through use of space–time rays and the (k, ω) dispersion surface in Fig. 2 (see [8, sec. 1.6]), with the radius of curvature R_c of the dispersion surface $ck(\omega)$ given by

$$R_c(\omega) = \{1 + [ck'(\omega)]^2\}^{3/2}/ck''(\omega). \tag{32}$$

For points near the beam axis, an approximate expression for the field in (24) can be obtained by expanding $\tilde{\Psi}(\mathbf{r},\, t;\, \boldsymbol{\xi},\, \overline{\boldsymbol{\xi}})$ in a Taylor series about $T = 0$ and $\boldsymbol{\xi} = \overline{\boldsymbol{\xi}}$. Truncating the expression after the quadratic term yields (only the $\boldsymbol{\xi}$ and T dependence is shown)

$$\tilde{\Psi}(T,\, \boldsymbol{\xi}) = \tilde{\Psi}_{00} + \tilde{\Psi}_{01}T + \tilde{\boldsymbol{\Psi}}_{01} \cdot (\boldsymbol{\xi} - \overline{\boldsymbol{\xi}}) + \tfrac{1}{2}\tilde{\Psi}_{20}T^2$$
$$+ \tilde{\boldsymbol{\Psi}}_{11}(\boldsymbol{\xi} - \overline{\boldsymbol{\xi}})T + \tfrac{1}{2}(\boldsymbol{\xi} - \overline{\boldsymbol{\xi}}) \cdot \tilde{\boldsymbol{\Psi}}_{02} \cdot (\boldsymbol{\xi} - \overline{\boldsymbol{\xi}}) + \cdots \tag{33}$$
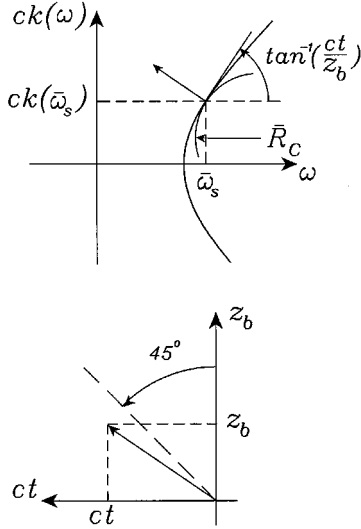
Fig. 2. On-axis PB asymptotics, dispersion surface and space–time rays. (a) $k(\omega)$ dispersion surface. The normal to the surface [see (31)] is parallel to the space–time ray to the observation point (z_b, ct). The construction determines the saddle-point values $\overline{\omega}_s(z, t)$ and $k[\overline{\omega}_s(z_b, t)]$. The local on-axis radius of curvature $\overline{R}_c$ of the dispersion curve is also shown [see (47)]. (b) Space–time ray to the observation point (z_b, ct).

where the Taylor coefficients are given by (see the Appendix)

$$\tilde{\Psi}_{00} \equiv \tilde{\Psi}|_{T=0, \boldsymbol{\xi}=\overline{\boldsymbol{\xi}}} = t\overline{\omega}_s - k(\overline{\omega}_s)z_b \qquad (34)$$

$$\tilde{\Psi}_{10} \equiv \partial_T \tilde{\Psi}|_{T=0, \boldsymbol{\xi}=\overline{\boldsymbol{\xi}}} = -\frac{i}{2}\overline{\omega}_s \qquad (35)$$

$$\tilde{\Psi}_{20} \equiv \partial_T^2 \tilde{\Psi}|_{T=0, \boldsymbol{\xi}=\overline{\boldsymbol{\xi}}} = [-4k''(\overline{\omega}_s)z_b]^{-1} \qquad (36)$$

$$\tilde{\boldsymbol{\Psi}}_{01} \equiv \nabla_{\boldsymbol{\xi}} \tilde{\Psi}|_{T=0, \boldsymbol{\xi}=\overline{\boldsymbol{\xi}}} = -k(\overline{\omega}_s)(\boldsymbol{x} - z\overline{\boldsymbol{\xi}}/\zeta) \qquad (37)$$

$$\tilde{\boldsymbol{\Psi}}_{11} \equiv \partial_T \nabla_{\boldsymbol{\xi}} \tilde{\Psi}|_{T=0, \boldsymbol{\xi}=\overline{\boldsymbol{\xi}}} = it(\boldsymbol{x} - z\overline{\boldsymbol{\xi}}/\zeta)/(2k''(\overline{\omega}_s)z_b^2) \qquad (38)$$

$$\tilde{\boldsymbol{\Psi}}_{02} \equiv \nabla_{\boldsymbol{\xi}} \nabla_{\boldsymbol{\xi}} \tilde{\Psi}|_{T=0, \boldsymbol{\xi}=\overline{\boldsymbol{\xi}}} = -k(\overline{\omega}_s)\boldsymbol{M} + \frac{t^2}{k''(\overline{\omega}_s)z_b^3}\boldsymbol{L} \qquad (39)$$

with

$$\boldsymbol{M} = \begin{bmatrix} i\beta - z(\overline{\xi}^2_1 + \overline{\zeta}^2)/\overline{\zeta}^3 & -z\overline{\xi}_1\overline{\xi}_2/\overline{\zeta}^3 \\ -z\overline{\xi}_1\overline{\xi}_2/\overline{\zeta}^3 & i\beta - z(\overline{\xi}_2^2 + \overline{\zeta}^2)/\overline{\zeta}^3 \end{bmatrix} \qquad (40)$$

and

$$\boldsymbol{L} = \begin{bmatrix} (x_1 + z\overline{\xi}_1/\overline{\zeta})^2 & (x_1 + z\overline{\xi}_1/\overline{\zeta})(x_2 + z\overline{\xi}_2/\overline{\zeta}) \\ (x_1 + z\overline{\xi}_1/\overline{\zeta})(x_2 + z\overline{\xi}_2/\overline{\zeta}) & (x_2 + z\overline{\xi}_2/\overline{\zeta})^2 \end{bmatrix}. \qquad (41)$$

Via the dependence on $\boldsymbol{x} - z\overline{\boldsymbol{\xi}}/\zeta$, these expressions make evident the skewing effect due to $\overline{\boldsymbol{\xi}} \neq 0$, when compared with the $\overline{\boldsymbol{\xi}} = 0$ results in [3].

2) Paraxial Approximation and its Domain of Validity: In view of (33), the phase $\tilde{\Psi}$ may be written in the form

$$\tilde{\Psi} = \tilde{\Psi}_p + \tilde{\Psi}_d \qquad (42)$$

where

$$\tilde{\Psi}_p = \left(t - \frac{i}{2}T\right)\overline{\omega}_s$$
$$- k(\overline{\omega}_s)\left[z_b + (\boldsymbol{x} - z\overline{\boldsymbol{\xi}}/\zeta)\cdot(\boldsymbol{\xi} - \overline{\boldsymbol{\xi}}) + \frac{1}{2}(\boldsymbol{\xi} - \overline{\boldsymbol{\xi}})\cdot\boldsymbol{M}\cdot(\boldsymbol{\xi} - \overline{\boldsymbol{\xi}})\right] \qquad (43)$$

is the *spectral paraxial* phase and

$$\tilde{\Psi}_d = \frac{1}{k''(\overline{\omega}_s)z_b}\left[-\frac{1}{8}T^2 + \frac{t^2}{2z_b^2}(\boldsymbol{\xi} - \overline{\boldsymbol{\xi}})\cdot\boldsymbol{L}\cdot(\boldsymbol{\xi} - \overline{\boldsymbol{\xi}})\right.$$
$$\left. + \frac{itT(\boldsymbol{x} - z\overline{\boldsymbol{\xi}}/\zeta)\cdot(\boldsymbol{\xi} - \overline{\boldsymbol{\xi}})}{2z_b}\right] \qquad (44)$$

is the nonparaxial term. Inserting (41) into (44) yields

$$\tilde{\Psi}_d = [2k''(\overline{\omega}_s)z_b]^{-1}\left[\frac{iT}{2} + \frac{t}{z_b}(\boldsymbol{\xi} - \overline{\boldsymbol{\xi}})\cdot(\boldsymbol{x} - z\overline{\boldsymbol{\xi}}/\zeta)\right]^2. \qquad (45)$$

Using (28), we obtain the paraxial approximation for the plane wave field

$$\overset{+}{\tilde{u}}(\boldsymbol{r}, t; \boldsymbol{\xi}, \overline{\boldsymbol{\xi}}) = \beta k(\overline{\omega}_s)[-2\pi iz_b k''(\overline{\omega}_s)]^{-1/2}$$
$$\cdot \exp[-i\tilde{\Psi}_p(\boldsymbol{r}, t; \boldsymbol{\xi}, \overline{\boldsymbol{\xi}})] \qquad (46)$$

where $\tilde{\Psi}_p$ is given in (43) and the amplitude term is obtained from (30), with the zero-order approximation, $T = 0, \boldsymbol{\xi} = \overline{\boldsymbol{\xi}}$.

We shall examine the parametric regimes for which $\tilde{\Psi}_d$ in (45) may be neglected, thereby furnishing a criterion for validity of the paraxial approximation. Utilizing the $k(\omega)$ dispersion surface and recalling (32) and (31) yields the radius of curvature $\overline{R}_c$ at $\overline{\omega}_s$ corresponding to the space–time *on-axis* observation point (z_b, t)

$$\overline{R}_c \equiv R_c(\overline{\omega}_s) = \frac{(1 + \overline{\Omega}^2)^{3/2}}{ck''(\overline{\omega}_s)}, \qquad \overline{\Omega} = \frac{ct}{z_b}. \qquad (47)$$

Note that $\overline{R}_c$ has the dimensionality $\omega \sim t^{-1}$ (see Fig. 2). Then from (45) and (47)

$$\tilde{\Psi}_d = \frac{c}{-2z_b}(1 + \overline{\Omega}^2)^{-3/2}|\overline{R}_c|$$
$$\cdot \left[-\frac{T}{2} - \frac{it}{z_b}(\boldsymbol{\xi} - \overline{\boldsymbol{\xi}})\cdot(\boldsymbol{x} - z\overline{\boldsymbol{\xi}}/\zeta)\right]^2. \qquad (48)$$

In view of (42), the nonparaxial term Ψ_d may be neglected when $|\Psi_d| \ll 2\pi$. To use this condition in a parametric estimate, we define a critical *on-axis* nondimensional estimator based on the equality $|\Psi_d| = 2\pi$ [note from (20) and (52) that for *on-axis* observation points, $\boldsymbol{x} = z\overline{\boldsymbol{\xi}}/\zeta$]

$$Q_T = |\Psi_d(\boldsymbol{\xi} = \overline{\boldsymbol{\xi}})|/(2\pi) = \frac{c}{16\pi z_b}(1 + \overline{\Omega}^2)^{-3/2}|\overline{R}_c|T^2. \qquad (49)$$

The condition $|\Psi_d| \ll 2\pi$, which validates the paraxial approximation in (43) *on-axis*, may now be stated as follows:

$$Q_T \ll 1. \qquad (50)$$

For a given space–time *on-axis* observation point, $\overline{R}_c$ is determined via (47), and (50) bounds the largest pulse length T, which is compatible with the paraxial approximation. Alternatively, keeping T constant, inequality (50) defines the maximum $\overline{\Omega} = ct/z_b$, i.e., the on-axis space–time region, for which the paraxial approximation is valid. Behind the wavefront, keeping z_b constant yields the maximum allowable observation time $t = \overline{\Omega}z_b/c$ while keeping t constant yields via (49) the maximum allowable $\overline{R}_c$ and the minimum allowable observer location $z_b = ct/\overline{\Omega}$. The estimates fail for observation points corresponding to $\overline{R}_c \to \infty$, i.e., $k''(\overline{\omega}_s) \to 0$. This happens near the first arrival of the signal $\overline{\Omega} \to 1$, where dispersion is not yet fully developed $(k(\omega) \to \omega/c)$ (see [1, eq. 28]) and also near inflection points

on the dispersion surface for complex materials. Better asymptotics than those based on (27) are required in these transition regions [2].

For *off-axis* observation points, we define an additional critical nondimensional estimator $Q_\xi \equiv |\Psi_d(T=0)|/(2\pi)$. Using (45) and (32) we obtain

$$Q_\xi = \frac{ct^2}{4\pi z_b^3} \left(1 + \overline{\Omega}^2\right)^{-3/2} |\overline{R}_c| |(\xi - \overline{\xi}) \cdot (\boldsymbol{x} - z\overline{\xi}/\overline{\zeta})|^2 \ll 1 \tag{51}$$

in which the estimator Q_ξ is evaluated in terms of the on-axis parameters $\overline{\Omega}$, $\overline{R}_c$, and z_b. To relate this expression to the beam coordinates in (20), we express $(\boldsymbol{x} - z\overline{\xi}/\overline{\zeta})$ in terms of the off-axis beam coordinates $\boldsymbol{x}_b$ using (20) as

$$(\boldsymbol{x} - z\overline{\xi}/\overline{\zeta}) = \begin{bmatrix} \cos \overline{\varphi}/\cos \overline{\vartheta} & -\sin \overline{\varphi} \\ \sin \overline{\varphi}/\cos \overline{\vartheta} & \cos \overline{\varphi} \end{bmatrix} \begin{bmatrix} x_{b1} \\ x_{b2} \end{bmatrix} \tag{52}$$

where $(\overline{\vartheta}, \overline{\varphi})$ are the spherical angles that define the beam direction $\overset{\circ}{\overline{\boldsymbol{\kappa}}} = (\overline{\xi}, \overline{\zeta})$ via (21). From (51), one has the following estimates.

1) The maximum excursion of ξ from $\overline{\xi}$ for a given off-axis observation point $(z_b, \boldsymbol{x}_b, t)$; this specifies the allowable angular spread that can be included when performing the transient plane wave superposition in (11) using the spectral paraxial phase in (43).

2) The maximum excursion $\boldsymbol{x}_b$ from the beam axis for given ξ; this is obtained by inserting (52) into (51). Moreover, for on-axis observation points $\boldsymbol{x}_b = 0$ it follows from (52) that $\boldsymbol{x} - z\overline{\xi}/\overline{\zeta} = 0$. Accordingly, on axis, the estimator $Q_\xi = 0$; off axis, the allowable maximum angular spread $\xi - \overline{\xi}$ decreases with distance from the beam axis. As in (49), Q_ξ is parameterized by the *on-axis* observation point (z_b, t) which determines, via $\overline{\Omega} = ct/z_b$, the location behind the wavefront and the local radius of curvature $\overline{R}_c$ of the dispersion surface.

The spectral function $\overset{+}{\tilde{u}}$ in (28) can be regarded either as a configuration-space object, where ξ is kept constant and the space–time observation point $(\boldsymbol{r}, t)$ is allowed to vary or as a spectral distribution, where $(\boldsymbol{r}, t)$ is kept constant and ξ is allowed to vary. Emphasizing the configurational domain, we consider the space–time behavior of a single dispersive spectral plane wave $\overset{+}{\tilde{u}}(\boldsymbol{r}, t; \xi, \overline{\xi}; T)$ propagating in the specified direction $\overset{\circ}{\boldsymbol{\kappa}} = (\xi, \zeta)$ [note from (26) with (25) that $\tilde{\omega}_s$ and, therefore, (28) with (29) and (30), are all functions of $\overset{\circ}{\boldsymbol{\kappa}} \cdot \boldsymbol{r} = \xi \cdot \boldsymbol{x} + \zeta z$]. The paraxially approximated form in (46) restricts the specified propagation angle to a direction close to the direction $\overset{\circ}{\overline{\boldsymbol{\kappa}}}$ of the beam axis [see (51)]. The spectral paraxial phase in (43) is in accord with the nondispersive paraxial delay obtained by second-order approximation of $\overset{\circ}{\boldsymbol{\kappa}} \cdot \boldsymbol{r}$ in (15) about $\xi = \overline{\xi}$. In view of (52), the term $(\boldsymbol{x} - z\overline{\xi}/\overline{\zeta})$ in the paraxial phase (43) vanishes for on-axis observation points where $\boldsymbol{x}_b = 0$. For off-axis observation points where $(\boldsymbol{x} - z\overline{\xi}/\overline{\zeta}) \neq 0$, additional phase is added to the on-axis phase by the linear term in $(\xi - \overline{\xi})$ in (43) as well as a second-order term due to the real part of $\boldsymbol{M}$. These additions adjust the on-axis parameter z_b so as to accommodate the exact plane wave constant delay surfaces $ct = \overset{\circ}{\boldsymbol{\kappa}} \cdot \boldsymbol{r}$ [as in (15)] up to second-order terms in $(\xi - \overline{\xi})$ [see (73) and (76)]. Note that

first-order changes in the phase due to the change in the spectral stationary frequency $\tilde{\omega}_s$ caused by an off-axis observation point are zero due to the definition of the spectral stationary frequency in (31) [see also (72)]. Therefore, the paraxial field in (46) is given in terms of the on-axis stationary frequency $\overline{\omega}_s$. The paraxial phase also includes the correction term $-i/2\overline{\omega}_s$ due to first-order change in the stationary frequency caused by the small parameter T [see (35)]. The paraxial phase neglects changes due to all *second-order* changes in the stationary frequency (∂_T^2, $\partial_{T\xi}$, and ∂_ξ^2). These phase changes are included in Ψ_d and may be neglected under conditions (50) and (51).

Emphasizing the spectral domain, we consider the directional behavior of the spectral plane waves $\overset{+}{\tilde{u}}$ arriving from different directions ξ at a fixed space–time point $(\boldsymbol{r}, t)$. Viewed from this perspective, the paraxial phase in (43) peaks at $\xi = \overline{\xi}$ and exhibits Gaussian decay for ξ away from $\overline{\xi}$ [recall that $\beta_r > 0$ in (40)]. This decay is due to the complex spectra in (8). The paraxial phase neglects second-order changes in ξ due to ξ-induced changes in the stationary frequency [recall from (26)] that $\tilde{\omega}_s$ is a function of ξ).

These considerations furnish insight into the contribution of the paraxial and nonparaxial phases to the space–time PB field in (11). Within the paraxial approximation in (46), the spectral superposition in (11) has the form of an inverse Fourier transform of a Gaussian in $(\xi - \overline{\xi})$. Therefore, the resulting PB field has the form of a Gaussian in the off-axis parameter in (52) [see also (62)]. For *on-axis* observation points $\boldsymbol{x}_b = 0$, the parameter Q_ξ in (51) vanishes, indicating that the paraxial approximation applies to *all* ξ values provided that (50) is satisfied. This is attributed to the fact that for $T = 0$, the nonparaxial phase term in (45), which quantifies the deviation of the stationary frequency $\tilde{\omega}_s$ from the on-axis frequency $\overline{\omega}_s$, vanishes on axis. Away from the beam axis, Q_ξ increases with $\boldsymbol{x}_b$ [see (51)] and the paraxial approximation is valid up to those $\boldsymbol{x}_b$ that satisfy $Q_\xi \approx 1$. Beyond this range, $\tilde{\Psi}_d$ has to be taken into account, in addition to $\tilde{\Psi}_p$. Under condition (50), the *nonparaxial* phase in (45) consists of a second order term in $(\xi - \overline{\xi})$ multiplied by a second-order term in $\boldsymbol{x}_b$ [see (45) with (52)]. Adding this term to the paraxial approximation in (43) and inserting into (11), we find that the resulting integral has the form of an inverse Fourier transform. The presence of $\boldsymbol{x}_b$ in $\tilde{\Psi}_d$ will result in a PB field having a *fourth order* term in the transverse coordinate $\boldsymbol{x}_b$ (a second-order term from the inversion of the Gaussian times the second-order coefficient in (52) (see also (63)]), thereby justifying the definitions in (43) and (45).

B. Asymptotic Evaluation of TD Spectral Integral

The formal representation of the TD field is given by the superposition integral in (11). For the spectral distribution in (28) this yields

$$\overset{+}{\tilde{u}}(\boldsymbol{r}, t) \sim \int d^2\xi \, \overset{+}{\tilde{A}}(\boldsymbol{r}, t; \xi) e^{-i\tilde{\Psi}}. \tag{53}$$

We shall evaluate (53) using the *paraxial* field in (46). Integral (53) has a stationary point ξ_s in the complex ξ domain that satisfies

$$\nabla_\xi \tilde{\Psi}_p(\xi)_{\xi = \xi_s} = 0, \qquad \xi_s = \xi_s(\boldsymbol{r}; \overline{\xi}; T). \tag{54}$$

The field may again be evaluated asymptotically via the lowest order two-dimensional saddle point formula [8, eq. 4.7.3]

$$u(\boldsymbol{r},\,t) \sim \overset{+}{A}(\boldsymbol{r},\,t;\,\overline{\boldsymbol{\xi}};\,T)e^{-i\Psi(\boldsymbol{r},\,t;\,\overline{\boldsymbol{\xi}})} \tag{55}$$

with

$$\Psi(\boldsymbol{r},\,t;\,\overline{\boldsymbol{\xi}};\,T) \equiv \tilde{\Psi}_p(\boldsymbol{r},\,t;\,\boldsymbol{\xi},\,\overline{\boldsymbol{\xi}};\,T)_{\overline{\boldsymbol{\xi}}=\boldsymbol{\xi}_s} \tag{56}$$

and

$$\overset{+}{A}(\boldsymbol{r},\,t;\,\overline{\boldsymbol{\xi}};\,T) = \overset{+}{A}(\boldsymbol{r},\,t;\,\boldsymbol{\xi},\,\overline{\boldsymbol{\xi}};\,T)|_{\boldsymbol{\xi}=\overline{\boldsymbol{\xi}}} \frac{-2\pi i}{[\text{Det} \, \nabla_{\xi}\nabla_{\xi}\tilde{\Psi}_p|\boldsymbol{\xi}_s]^{1/2}}. \tag{57}$$

Since the fields in the integrand are approximated by their paraxial (quadratic) form, the integration can be performed exactly.

1) Stationary Point: Inserting (43) into (54) yields

$$\nabla_{\xi}[z_b + (\boldsymbol{x} - z\overline{\boldsymbol{\xi}}/\zeta) \cdot (\boldsymbol{\xi} - \overline{\boldsymbol{\xi}})$$
$$+ \tfrac{1}{2}(\boldsymbol{\xi} - \overline{\boldsymbol{\xi}}) \cdot \boldsymbol{M} \cdot (\boldsymbol{\xi} - \overline{\boldsymbol{\xi}})]_{\boldsymbol{\xi}=\boldsymbol{\xi}_s} = 0 \tag{58}$$

and, therefore,

$$\boldsymbol{\xi}_s = \overline{\boldsymbol{\xi}} - \boldsymbol{M}^{-1} \cdot (\boldsymbol{x} - z\overline{\boldsymbol{\xi}}/\zeta). \tag{59}$$

From (59) we note that the displacement of $\boldsymbol{\xi}_s$ from the on-axis real value $\overline{\boldsymbol{\xi}}$ is proportional to $(\boldsymbol{x} - z\overline{\boldsymbol{\xi}}/\zeta)$ and, therefore, via (52) to $\boldsymbol{x}_b$.

2) Phase Ψ: The phase Ψ is obtained by inserting (59) into (56)

$$\Psi(\boldsymbol{r},\,t) = \left(t - \frac{i}{2}T\right)\overline{\omega}_s$$
$$- k(\overline{\omega}_s)\left[z_b - \tfrac{1}{2}(\boldsymbol{x} - z\overline{\boldsymbol{\xi}}/\zeta) \cdot \boldsymbol{M}^{-1} \cdot (\boldsymbol{x} - z\overline{\boldsymbol{\xi}}/\zeta)\right]. \tag{60}$$

Utilizing the beam coordinates in (20) as well as relation (52) we find that

$$-(\boldsymbol{x} - z\overline{\boldsymbol{\xi}}/\zeta) \cdot \boldsymbol{M}^{-1} \cdot (\boldsymbol{x} - z\overline{\boldsymbol{\xi}}/\zeta) = \boldsymbol{x}_b \cdot \boldsymbol{Q} \cdot \boldsymbol{x}_b \tag{61}$$

where $\boldsymbol{Q}$ is given by (19) and the paraxial phase may be expressed in terms of the beam coordinates

$$\Psi(\boldsymbol{r},\,t) = \left(t - \frac{i}{2}T\right)\overline{\omega}_s - k(\overline{\omega}_s)\left[z_b + \frac{1}{2}\boldsymbol{x}_b \cdot \boldsymbol{Q} \cdot \boldsymbol{x}_b\right]. \tag{62}$$

The phase in (62) consists of the on-axis phase $\overline{\omega}_s(t - (iT/2)) - k(\overline{\omega}_s)z_b$ and an additional paraxial off-axis term $(1/2)\boldsymbol{x}_b \cdot \boldsymbol{Q} \cdot \boldsymbol{x}_b$ [cf. (18) and (23)]. The result in (62) is valid as long as T satisfies condition (50) and as long as the stationary point $\boldsymbol{\xi}_s$ satisfies condition (51). Using (59), we find that $\boldsymbol{\xi}_s - \overline{\boldsymbol{\xi}} = \boldsymbol{M}^{-1} \cdot (\boldsymbol{x} - z\overline{\boldsymbol{\xi}}/\zeta)$ and substituting into (51) we obtain

$$Q_{\boldsymbol{x}_b} \equiv \frac{ct^2}{4\pi z_b^3}(1 + \overline{\Omega}^2)^{-3/2}|\overline{R}_c||\boldsymbol{x}_b \cdot \boldsymbol{Q} \cdot \boldsymbol{x}_b|^2 \ll 1 \tag{63}$$

where $Q_{\boldsymbol{x}_b}$ is the critical nondimensional estimator that parameterizes the maximum off-axis excursion $\boldsymbol{x}_b$ for which the paraxial phase in (62) is valid, i.e., the maximum off-axis excursion $\boldsymbol{x}_{b_{\max}}$ is obtained for $Q_{\boldsymbol{x}_b} \simeq 1$. For a nondispersive field, this deviation is parameterized by $|\boldsymbol{x}_b| \ll z_b$ alone. When dispersion is introduced, the parameters $\overline{R}_c$ and $\overline{\Omega}$ play a role in addition to z_b. However, the estimate in (63) becomes

invalid when $|\overline{R}_c| \to \infty$ because the amplitude in (46) shows that the asymptotic field amplitude diverges in that limit [see also the amplitude in (64); for a uniform correction when $\overline{\boldsymbol{\xi}} = 0$, see [2]].

3) Amplitude $\overset{+}{A}$: Inserting (39) together with (30) into (57) yields

$$\overset{+}{A}(\boldsymbol{r},\,t) = \sqrt{\frac{2}{i\pi z_b k''(\overline{\omega}_s)}}\sqrt{\frac{\det \boldsymbol{Q}(z)}{\det \boldsymbol{Q}(0)}}. \tag{64}$$

Comparing this result with the one found in [1, eq. (57)], we find that by setting $S = z + \boldsymbol{x}^2/(z - i\beta) \to z$ in [1, eq. (57)], the two results are identical for the special case $\overline{\boldsymbol{\xi}} = 0$. Therefore, the generalized result in (64) is the zeroth-order off-axis $\boldsymbol{x}$ term of [1, eq. (57)], a common approximation for the amplitude.

The paraxial dispersive PB field in (55) with (62) and (64) can be parameterized in terms of beam widths, wave front radii of curvature, instantaneous frequencies, etc., by using the field envelope and paraxial phase in the manner established in [2] for the normally $(\overline{\boldsymbol{\xi}} = 0)$ propagating beam. We shall not pursue this line of investigation here.

V. CONCLUSION

In this paper, we have formulated and asymptotically evaluated a direct TD spectral analysis and synthesis procedure for the propagation of a paraxial PB launched obliquely from a hypothetical aperture plane into a lossless homogeneous unbounded dispersive medium characterized by the generic dispersion relation $k(\omega)$. Various critical nondimensional estimators have been shown to play an important role in quantifying the range of validity of the paraxial approximation. Procedural details have been summarized in Section I and need not be repeated here. We conclude with the observation that the new results developed in this paper permit the asymptotic representation, via PB superposition [6], of fields excited by *arbitrary* short-pulse initial source distributions in the dispersive environment. Extension of these techniques to lossy dispersive materials is under consideration.

APPENDIX
DERIVATION OF (34)–(41)

In order to evaluate the Taylor coefficients in (33), we note that

$$\tilde{\omega}_s|_{T=0,\,\boldsymbol{\xi}=\overline{\boldsymbol{\xi}}} = \overline{\omega}_s, \qquad \tilde{S}|_{\boldsymbol{\xi}=\overline{\boldsymbol{\xi}}} = \overset{\circ}{\boldsymbol{\kappa}} \cdot \boldsymbol{r} = z_b. \tag{65}$$

1) Ψ_{00}: Sampling $\tilde{\Psi}$ in (29) at $T = 0$ and $\boldsymbol{\xi} = \overline{\boldsymbol{\xi}}$, and using (65) we obtain (34).

2) Ψ_{10}: Using (29) one finds (only the T dependence is shown)

$$\partial_T \tilde{\Psi}(T) = -\frac{i}{2}\tilde{\omega}_s(T) + \left(t - \frac{i}{2}T\right)\partial_T\tilde{\omega}_s(T) - \tilde{S}\partial_T k[\tilde{\omega}_s(T)] \tag{66}$$

where $\partial_T = \partial/\partial T$. Using

$$\tilde{S}\partial_T k[\tilde{\omega}_s(T)] = \tilde{S}k'[\tilde{\omega}_s(T)]\partial_T\tilde{\omega}_s(T) = \left(t - \frac{i}{2}T\right)\partial_T\tilde{\omega}_s(T) \tag{67}$$

in (66) leads to

$$\partial_T \tilde{\Psi}(T) = -\frac{i}{2} \tilde{\omega}_s(T) \tag{68}$$

with the last equality in (67) obtained from (26). Sampling (68) at $T = 0$, $\xi = \overline{\xi}$ yields $\check{\Psi}_{10}$ in (35).

3) Ψ_{20}: Applying ∂_T to (26) we find (only the T dependence is shown)

$$\partial_T \tilde{\omega}_s(T) = \frac{-i}{2\tilde{S}k''[\tilde{\omega}_s(T)]} \tag{69}$$

and $\partial_T^2 \tilde{\Psi}$ is evaluated using (68)

$$\partial_T^2 \tilde{\Psi}(T) = -\frac{i}{2} \partial_T \tilde{\omega}_s(T) = \frac{1}{-4\tilde{S}k''[\tilde{\omega}_s(T)]}. \tag{70}$$

The final expression in (36) follows via (65) and (70).

4) $\tilde{\Psi}_{01}$: Using (29) we obtain (only the ξ dependence is shown)

$$\nabla_\xi \tilde{\Psi}(\xi) = \left(t - \frac{i}{2}T\right)\nabla_\xi \tilde{\omega}_s(\xi) - \tilde{S}(\xi)\nabla_\xi k[\tilde{\omega}_s(\xi)]$$
$$- k[\tilde{\omega}_s(\xi)]\nabla_\xi \tilde{S}(\xi) \tag{71}$$

and $\nabla_\xi k(\tilde{\omega}_s)$ is evaluated using (26)

$$\nabla_\xi k[\tilde{\omega}_s(\xi)] = k'[\tilde{\omega}_s]\nabla_\xi \tilde{\omega}_s(\xi) = \frac{t - \frac{i}{2}T}{\tilde{S}(\xi)}\nabla_\xi \tilde{\omega}_s(\xi). \tag{72}$$

Inserting (72) into (71) yields

$$\nabla_\xi \tilde{\Psi}(\xi) = -k(\tilde{\omega}_s)\nabla_\xi \tilde{S}(\xi)$$
$$= -k(\tilde{\omega}_s)[\boldsymbol{x} - z\boldsymbol{\xi}/\zeta + i\beta(\boldsymbol{\xi} - \overline{\boldsymbol{\xi}})] \tag{73}$$

where the last equality was obtained taking $\tilde{S}$ from (25), as well as $\nabla \overset{\circ}{\boldsymbol{\kappa}} \cdot \boldsymbol{r} = \nabla(\boldsymbol{\xi} \cdot \boldsymbol{x} + \sqrt{1 - \xi^2}z) = \boldsymbol{x} - z\boldsymbol{\xi}/\zeta$. The final result in (37) is obtained using (65) in (73).

5) $\tilde{\Psi}_{11}$: Applying ∂_T to (73) yields (note that in (73) only $\tilde{\omega}_s$ is a function of T)

$$\partial_T \nabla_\xi \tilde{\Psi} = -k'[\tilde{\omega}_s(T)][\boldsymbol{x} - z\boldsymbol{\xi}/\zeta + i\beta(\boldsymbol{\xi} - \overline{\boldsymbol{\xi}})]\partial_T \tilde{\omega}_s(T)$$
$$= it[\boldsymbol{x} - z\boldsymbol{\xi}/\zeta + i\beta(\boldsymbol{\xi} - \overline{\boldsymbol{\xi}})]/[2\tilde{S}^2 k''(\tilde{\omega}_s)]. \tag{74}$$

The last equality is obtained from (26) and (69), and the final result in (38) follows from (65) and (74).

6) $\tilde{\Psi}_{02}$: Denoting $\partial_l = \partial/\partial_{\xi_l}$, $l = 1, 2$, we rewrite (73) in the form

$$\partial_l \tilde{\Psi}(\xi) = -k[\tilde{\omega}_s(\xi)](x_l - z\xi_l/\zeta) - k[\tilde{\omega}_s(\xi)]i\beta(\xi_l - \overline{\xi}_l) \tag{75}$$

and, therefore,

$$\partial_m \partial_l \tilde{\Psi} = -k(\tilde{\omega}_s)\partial_m[(x_l - z\xi_l/\zeta) + i\beta(\xi_l - \overline{\xi}_l)]$$
$$- [x_l - z\xi_l/\zeta + i\beta(\xi_l - \overline{\xi}_l)]\partial_m k[\tilde{\omega}_s(\xi)]. \tag{76}$$

To simplify this expression we use (31)

$$\partial_m k[\tilde{\omega}_s(\xi)] = k'[\tilde{\omega}_s(\xi)]\partial_m \tilde{\omega}_s(\xi) = \frac{t - \frac{i}{2}T}{\tilde{S}}\partial_m \tilde{\omega}_s(\xi) \tag{77}$$

and evaluate $\partial_m \tilde{\omega}_s(\xi)$ by applying ∂_m to (26), giving

$$\partial_m \tilde{\omega}_s(\xi) = \frac{-1}{k''(\tilde{\omega}_s)\tilde{S}^2(\xi)}\left(t - \frac{i}{2}T\right)\partial_m \tilde{S}(\xi)$$
$$= \frac{-\left(t - \frac{i}{2}T\right)(x_m - z\xi_m/\zeta - i\beta(\xi_m - \overline{\xi}_m))}{k''(\tilde{\omega}_s)\tilde{S}^2}. \tag{78}$$

Using (77) and (78) in (76) and evaluating the ∂_m derivatives in (76) yields (39).

REFERENCES

[1] T. Melamed and L. B. Felsen, "Pulsed beam propagation in lossless dispersive media: Part I—Theory," *J. Opt. Soc. Amer. A*, vol. 15, pp. 1268–1276, 1998.

[2] ——, "Pulsed beam propagation in lossless dispersive media: Part II—A numerical example," *J. Opt. Soc. Amer. A*, vol. 15, pp. 1277–1284, 1998.

[3] ——, "Pulsed beam propagation in lossless dispersive media," in *Ultra-Wideband, Short-Pulse Electromagnetics*. New York: Plenum, 1999.

[4] E. Heyman and T. Melamed, "Certain considerations in aperture synthesis of ultrawideband/short-pulse radiation," *IEEE Trans. Antennas Propagat.*, vol. 42, pp. 518–525, Apr. 1994.

[5] B. Z. Steinberg, E. Heyman, and L. B. Felsen, "Phase-space beam summation for time dependent radiation from large apertures: Continuous parametrization," *J. Opt. Soc. Amer. A*, vol. 8, pp. 943–958, 1991.

[6] T. Melamed, "Phase-space beam summation: A local spectrum analysis for time-dependent radiation," *J. Electromagn. Waves Applicat.*, vol. 11, pp. 739–773, 1997.

[7] E. Heyman, "Pulsed beam propagation in an inhomogeneous medium," *IEEE Trans. Antennas Propagat.*, vol. 42, pp. 311–319, Mar. 1994.

[8] L. B. Felsen and N. Marcuvitz, *Radiation and Scattering of Waves*. Piscataway, NJ: IEEE Press, 1994.

Timor Melamed was born is Tel-Aviv, Israel, in January 1964. He received the B.Sc. degree (*magma cum laude*) in electrical engineering and the Ph.D. degree, both from Tel-Aviv University, Israel, in 1989 and 1997, respectively.

From 1989 to 1990, he worked on microprocessors design at National Semiconductor, Tel Aviv, Israel. From 1996 to 1998 he held a postdoctoral position at the Department of Aerospace and Mechanical Engineering, Boston University, MA. He is currently with Odin Technologies, Yokne'am Elit, Israel. His main fields of interest are analytic techniques in wave theory, transient wave phenomena, and inverse scattering.

Leopold B. Felsen (S'47–M'54–SM'55–F'62–LF'90) was born in Munich, Germany, on May 7, 1924. He received the B.E.E., M.E.E, and D.E.E. degrees from the Polytechnic Institute of Brooklyn, Brooklyn, NY, in 1948, 1950, and 1952, respectively.

He emigrated to the United States in 1939 and served in the U.S. Army from 1943 to 1946. After 1952 he remained with the Polytechnic (now Polytechnic University), gaining the position of University Professor in 1978. From 1974 to 1978 he was Dean of Engineering. In 1994 he resigned from the full-time Polytechnic faculty and was granted the status of University Professor Emeritus. He is now Professor of Aerospace and Mechanical Engineering and Professor of Electrical and Computer Engineering at Boston University, Boston, MA. He is the author or coauthor of over 300 papers and of several books, including the classic *Radiation and Scattering of Waves* (Piscataway, NJ: IEEE Press, 1994). He is an associate editor of several professional journals and an editor of the *Wave Phenomena Series* (New York: Springer-Verlag). His research interests encompass wave propagation and diffraction in complex environments and in various disciplines, high-frequency asymptotic and short-pulse techniques, and phase-space methods with an emphasis on wave-oriented data processing and imaging.

Dr. Felsen is a member of Sigma Xi and a Fellow of the Optical Society of America and the Acoustical Society of America. He has held named Visiting Professorships and Fellowships at universities in the United States and abroad, including the Guggenheim in 1973 and the Humboldt Foundation Senior Scientist Award in 1981. In 1974 he was an IEEE/APS Distinguished Lecturer. He was awarded the Balthasar van der Pol Gold Medal from the International Union of Radio Science (URSI) in 1975, an honorary doctorate from the Technical University of Denmark in 1979, the IEEE Heinrich Hertz Gold Medal for 1991, the APS Distinguished Achievement Award for 1998, the IEEE Third Millenium Medal in 2000 (nomination by APS), three Distinguished Faculty Alumnus Awards from Polytechnic University, and an IEEE Centennial Medal in 1984. Also, awards have been bestowed on several papers authored or coauthored by him. In 1977 he was elected to the National Academy of Engineering. He has served as Vice Chairman and Chairman for both the United States and the International URSI Commission B.